

**Polar polymer-solvent interaction derived favorable interphase for stable lithium metal batteries**

Journal:	<i>Energy & Environmental Science</i>
Manuscript ID	EE-COM-08-2019-002558.R1
Article Type:	Communication
Date Submitted by the Author:	10-Sep-2019
Complete List of Authors:	Bae, Jiwoong; The University of Texas at Austin, Mechanical Engineering Qian, Yumin; University of Texas at Austin Li, Yutao; The University of Texas at Austin, Texas Materials Institute Zhou, Xingyi; The University of Texas at Austin, Materials Science and Engineering Goodenough, John; University of Texas at Austin, Center for Materials Sci and Eng Yu, Guihua; The University of Texas at Austin, Materials Science and Engineering

COMMUNICATION

Polar polymer-solvent interaction derived favorable interphase for stable lithium metal batteries

Jiwoong Bae, Yumin Qian, Yutao Li, Xingyi Zhou, John B. Goodenough, and Guihua Yu*

Received 00th January 20xx,
Accepted 00th January 20xx

DOI: 10.1039/x0xx00000x

Lithium metal has long been regarded as one of the most promising anode materials for future rechargeable batteries. However, the severe reaction of Li with carbonate electrolytes and the rapid growth of the Li-dendrite at high current densities hinder its practical application in Li-metal batteries. Here we report a polar polymer protective layer to suppress highly corrosive cyclic carbonates by tuning polymer-solvent interactions. The C≡N groups of the polyacrylonitrile (PAN) polymer chains in the polar polymer network can effectively reduce the high reactivity of the C=O groups of the carbonate solvents leading to a stable solid electrolyte interphase (SEI) layer with higher inorganic components. In-situ optical and electron microscopes demonstrate that the polar polymer network effectively restrained the formation and growth of Li-dendrite, which helps to stabilize the plating/stripping behavior of Li in a symmetric Li | Li cell and a Li | LiNi_{1/3}Co_{1/3}Mn_{1/3}O₂ cell. This study provides a useful perspective of controlling electrolyte coordination to form a stable SEI layer in carbonate electrolytes for Li-metal batteries.

Lithium (Li) metal, which has the highest theoretical capacity (3,860 mAh g⁻¹) and the lowest electrochemical potential (-3.04 V vs standard hydrogen electrode), has been regarded as a promising anode material for energy storage systems.¹ In the past decades, much effort has been devoted to exploring Li-metal as the anode for rechargeable batteries.²⁻⁶ In spite of all the endeavors, the high reactivity of carbonates (especially cyclic carbonate) hinders their application to Li-metal batteries, since carbonyl groups (C=O) often cause the decomposition of solvents, leading to a solvent-induced solid electrolyte interphase (SEI) layer.⁷ Such SEI layer has a chemical heterogeneity with a majority of organic components and is often accompanied by breakage and dissolution of the layer. The defected SEI layer no longer protects Li-metal, consuming

Broader context

Energy-dense, long-lasting rechargeable batteries are one of the urgent requirements for fast-growing electronic products such as portable electronics, electric vehicles, or smart grids. In order to increase the energy density of lithium ion batteries, various materials have been studied in which lithium (Li) metal attracts much attention as the future anode due to its high theoretical capacity (3,860 mAh g⁻¹) and low electrochemical potential (-3.04 V relative to standard hydrogen electrode). Nevertheless, the high reactivity of Li-metals and electrolytes often results in unstable interphase layers resulting in excessive Li dendrite formation. Such dendrite can form an inactive dead Li layer and lower the charge-discharge efficiency. In this study, we designed a polar polymer network on Li-metal that actively inhibits highly corrosive electrolytes by polar polymer-solvent interactions. As a result, Li-metal without dendrite can be rendered during the repeated plating / stripping process. Li-metal batteries with a practical cathode (LiNi_{1/3}Co_{1/3}Mn_{1/3}O₂) showed a good cycling stability of 94.0% capacity retention after 450 cycles at 1C and 98.7% after 1000 cycles at 5C.

more electrolyte and Li, and thus leads to a poor Coulombic efficiency, and eventually, to a cell failure (either short-circuiting or large impedance).²

Recently, various strategies have been proposed to stabilize Li-metal in carbonate electrolytes.⁸⁻¹³ One of the effective approaches is controlling the SEI layer either by an artificial SEI layer or electrolyte additives. An artificial SEI layer formed by *ex-situ* deposition of desired materials⁹ or *in-situ* reaction during the cycling^{10, 11} allows Li⁺ ion transport while blocks electron conduction, and therefore protecting Li-metal from the reactive electrolyte. Similarly, electrolyte additives such as 0.05M LiPF₆ or LiNO₃ have been also investigated to control the chemical composition of the SEI layer and to help a stable Li plating/stripping.^{12, 13} Despite considerable progress in engineering SEI layers, it still remains a challenge to satisfy high-power applications. Although above mentioned strategies are

^a Materials Science and Engineering Program and Department of Mechanical Engineering, The University of Texas at Austin, Austin, TX 78712, USA. Email: ghyu@austin.utexas.edu (G.Y.)

†Electronic Supplementary Information (ESI) available. See DOI: 10.1039/x0xx00000x

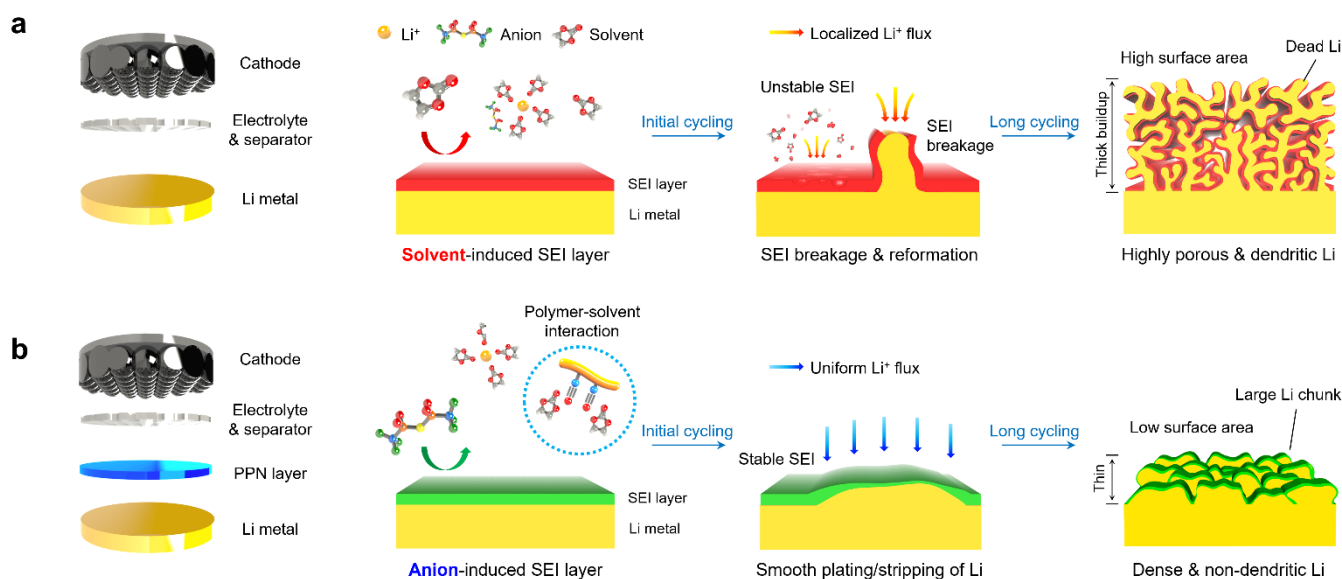


Fig. 1 Schematic illustration of the effect of PPN protective layer. (a) Solvent-induced SEI layer formation on the bare Li, which repeats during the cycling due to the defects of SEI layer. (b) Anion-induced SEI layer formation on PPN Li that effectively stabilizes Li surface during the cycling.

useful, a significant volume change of Li-metal under a high current density (1 mA cm^{-2}) may still cause breakage of SEI layer and evolution of Li dendrites (or buildup of dead Li), which results in shortened lifespan of Li-metal batteries. Therefore, a more reliable and active approach is required to intrinsically stabilize highly reactive electrolyte with Li-metal under a fast charging/discharging process.

In this study, we have developed a polar polymer network on Li-metal to reduce the reactivity of carbonate solvents by polymer-solvent interaction. The polar polymer protected Li leads to a stable SEI layer formation due to the reduced availability of free solvent molecules, but with more contribution from salt anions (e.g., PF_6^- or TFSI^-) as a precursor for inorganic components. Electrochemical analysis and *in-situ* optical microscopy prove that the polymer protected Li renders a stable Li plating/stripping while bare Li shows drastic growth of Li-dendrites and eventually ends with abundant dead Li. The polar polymer protected Li-metal battery with a $\text{LiNi}_{1/3}\text{Co}_{1/3}\text{Mn}_{1/3}\text{O}_2$ (NCM) cathode achieved an improved cyclability of 94.0% capacity retention after 450 cycles at 1C and 98.7% after 1000 cycles at 5C, indicating that Li-metal can be effectively stabilized in the carbonate electrolyte.

Polymer-solvent interaction in polar polymer network

In a conventional carbonate electrolyte, abundant carbonate solvents on the exposed surface of Li-metal rapidly decompose and react with Li, and thus form a solvent-induced SEI layer (Fig. 1a). This soluble and heterogeneous organic SEI layer is difficult to stabilize the Li-metal surface.¹⁴ The rupture of the SEI layer by volume change of Li-metal or dissolution of organic

component re-exposes the fresh Li to the electrolyte, leading to the dendrite growth and reformation of SEI layer. Such process is repeated and results in highly porous and dendritic Li buildup.

On the other hand, polymer-solvent interactions in the polar polymer network (PPN) can greatly reduce the reactivity and availability of carbonate solvents by dipole-dipole interaction between $\text{C}=\text{O}$ (from carbonate solvent) and $\text{C}\equiv\text{N}$ (from polar polymer) groups, while facilitating salt anions (e.g., PF_6^- or TFSI^-) to contribute to inorganic component of SEI layer, such as LiF (Fig. 1b).^{15, 16} The more inorganic components in SEI layer are hard to be dissolved compared to the organic components, and thus improving the chemical stability of SEI layer. The stable anion-induced SEI layer at the interface between PPN and Li-metal can prevent further reaction of the electrolyte with Li, and therefore enabling an effective Li plating/stripping. Furthermore, homogeneous SEI layer may guide uniform Li^+ ion flux which leads to dense Li morphology. Due to this smooth plating/stripping of Li, SEI breakage can be also avoided which prevents dendrite growth or further consumption of Li and electrolyte. The PPN layer is not decomposed or consumed by the reaction, but only creates chemical environment for electrolyte to form a stable SEI layer. Therefore, this method is reliable and sustainable compared to other passive strategies, such as an artificial SEI layer or an electrolyte additive that cannot fully recover the stable interfacial layer once it is destroyed.

To exploit the polymer-solvent interaction, PPN was designed by fabricating a semi-interpenetrating polymer network to embed polyacrylonitrile (PAN) polymer chains which have rich polar $\text{C}\equiv\text{N}$ groups for dipole-dipole interactions (Fig. 2a). The cross-linkable oligomers (i.e., polyethylene glycol diacrylate (PEGDA)) and PAN polymers are dissolved in the

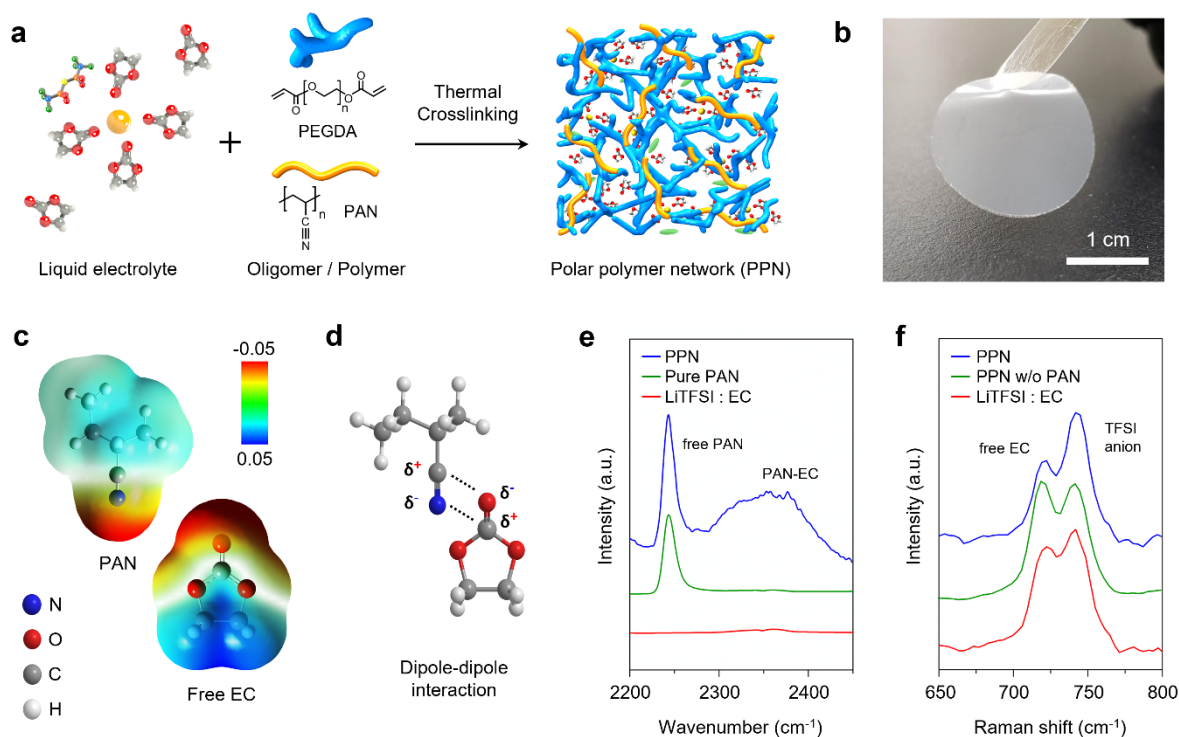


Fig. 2 Synthesis and characterization of PPN. (a) Schematic illustration of fabrication process of PPN. (b) Photograph of a PPN film. (c) Electrostatic potential maps of PAN and EC and (d) schematic illustration of dipole-dipole interaction between C≡N and C=O groups of PAN and EC, respectively. (e) FTIR spectra of PPN (blue), pure PAN (green) and LiTFSI : EC (red). (f) Raman spectra of PPN with (blue) and without PAN (green) and LiTFSI : EC (red).

desired liquid electrolyte. After thermally cross-linked, the PEGDA forms a three-dimensional (3D) polymer network where the PAN polymers are uniformly confined (Fig. 2b). With such design, PAN can interact effectively with the carbonate electrolyte and avoid direct contact with Li-metal.

Among many carbonate solvents, ethylene carbonate (EC) has been selected as a representative carbonate solvent, which is well-known for its high reactivity with Li.¹⁷ To investigate the dipole-dipole interaction, electrostatic potential maps were overlaid on the chemical structure of PAN and free EC as shown in Fig. 2c. The negative charge (red) is localized on the nitrogen of C≡N group of PAN and oxygen of C=O group of EC, respectively. Meanwhile, the charges on the carbons of C≡N and C=O groups are delocalized leading to a relatively positive charge. Due to these local dipoles caused by different charge densities, a C≡N group of PAN and a C=O group of EC strongly interact with each other forming a dipole-dipole interaction (Fig. 2d).¹⁸

The PAN-EC interaction and its influence on the electrolyte coordination were investigated by Fourier-transform infrared (FTIR) and Raman spectroscopy. To clearly demonstrate the polymer-solvent interaction (i.e., PAN-EC), PPN was fabricated in lithium bis(trifluoromethanesulfonyl)imide (LiTFSI) : EC electrolyte with the molar ratio of 1 : 6 which has the low melting point and the high conductivity.¹⁹ The FTIR spectrum shown in Fig. 2e displays clear evidence of polymer-solvent interaction by an additional band around 2350 cm⁻¹ for PPN (blue) which is known for PAN-EC interaction.^{18, 20} Meanwhile,

pure PAN (green) and LiTFSI : EC (red) do not show any band around 2350 cm⁻¹, confirming PAN-EC interaction only exists in PPN. Neither peak shift nor additional peak was observed related to free PAN peak around 2240 cm⁻¹ indicating that Li⁺ ions do not prefer to coordinate with PAN.²¹

To explore the influence of PAN-EC interaction on the electrolyte coordination, Raman spectroscopy was conducted with three different samples; PPN, PPN without PAN (PPN w/o PAN) and LiTFSI : EC (Fig. 2f). Strong salt anion (TFSI⁻) bands around 740-750 cm⁻¹ were observed through all samples which correspond to a common solvent-separated ion pair.²² With absence of PAN, free EC bands near 720 cm⁻¹ with a high intensity were also found for PPN w/o PAN and LiTFSI : EC implying plentiful uncoordinated EC molecules.¹⁹ In contrast, PPN shows a smaller intensity of free EC peak, from which it can be speculated that the strong PAN-EC interaction in PPN decreases the number of free EC molecules. For quantitative analysis, the ratio of free EC to LiTFSI bands was calculated where PPN shows the area ratio of 0.49 which is lower than that of LiTFSI : EC (0.67) or PPN w/o PAN (1.04) (Fig. S1, ESI[†]). Thermogravimetric analysis (TGA) and differential scanning calorimetry (DSC) also confirm that the coordination of EC in the PPN has changed compared to liquid phase solution (Fig. S2 and S3, ESI[†]).¹⁹ Based on FTIR and Raman spectroscopies, it can be concluded that C≡N groups of PAN polymer chains weakly

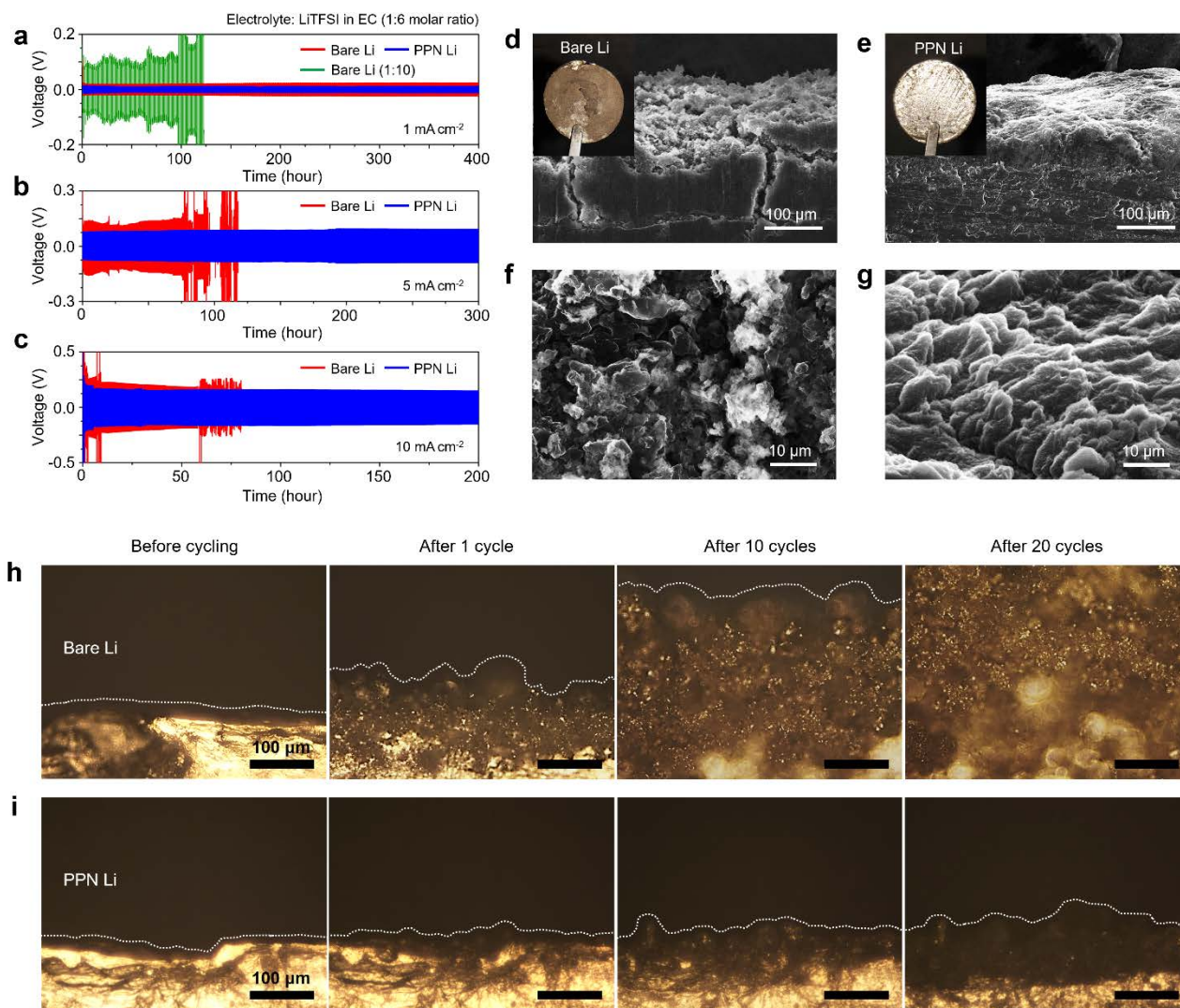


Fig. 3 Li plating/stripping behavior. Symmetric Li | Li cell cycling tests under different current densities of (a) 1 mA cm⁻², (b) 5 mA cm⁻² and (c) 10 mA cm⁻² for 1 mAh cm⁻². Cross-sectional SEM images of (d) bare Li and (e) PPN Li after cycling under 5 mA cm⁻². The inset shows the Li chip after cycling. SEM images of the top surface of (f) bare Li and (g) PPN Li after cycling under 5 mA cm⁻². *In-situ* observation of (h) bare Li and (i) PPN Li during Li plating/stripping process at 5 mA cm⁻² for 1 mAh cm⁻² up to 20 cycles.

interact with Li⁺ ions or TFSI anions, but solely and strongly interact with EC molecules.

Morphology and performance of Li plating/stripping

Electrochemical behavior of Li plating/stripping have been investigated with symmetric Li | Li cells under different current densities (Fig. 3). To see the distinctive role of PPN, EC single solvent-based electrolytes (LiTFSI : EC = 1 : 6) were used due to their high reactivity. As shown in Fig. 3a, bare Li cell with a dilute electrolyte (LiTFSI : EC = 1 : 10) demonstrates the worst cycling performance with an unstable overpotential (> 200 mV) under 1 mA cm⁻². The abundant free EC molecules could have reacted drastically with Li leading to an unstable interface. On the other hand, the electrolyte with a higher concentration (LiTFSI : EC = 1 : 6) showed a stable cycling with a small overpotential (~20 mV).^{23, 24} However, the voltage profiles become unstable under

the higher current densities (5 and 10 mA cm⁻²) as shown in Fig. 3b and 3c, indicating that high concentrations are not an effective mean to suppress the reactive EC solvents and Li-dendrites. By contrast, Li-metal surface stabilized by PPN (blue) demonstrates a stable cycling over 300 hrs under 5 mA cm⁻² and 200 hrs under 10 mA cm⁻² (Fig. 3b and 3c).

The morphology of Li was examined by scanning electron microscopy (SEM) (Fig. 3d-g). A highly porous surface with severe cracks was observed in bare Li (Fig. 3d). The photograph of the Li chip (inset of Fig. 3d) suggests that the Li surface is mostly composed of dead Li. Dendrites can also be found on the surface of Li in Fig. 3f implying a poor interfacial stability of bare Li (See also Fig. S4 for enlarged image, ESI[†]). For PPN Li, a relatively clean Li chip was obtained from the disassembled cell (inset of Fig. 3e). The SEM images also present a dendrite-free and highly dense morphology without any crack (Fig. 3e and g). Li electroplating as also conducted under 1 mA cm⁻² for 2 hrs to see the initial Li deposition morphology which confirms that

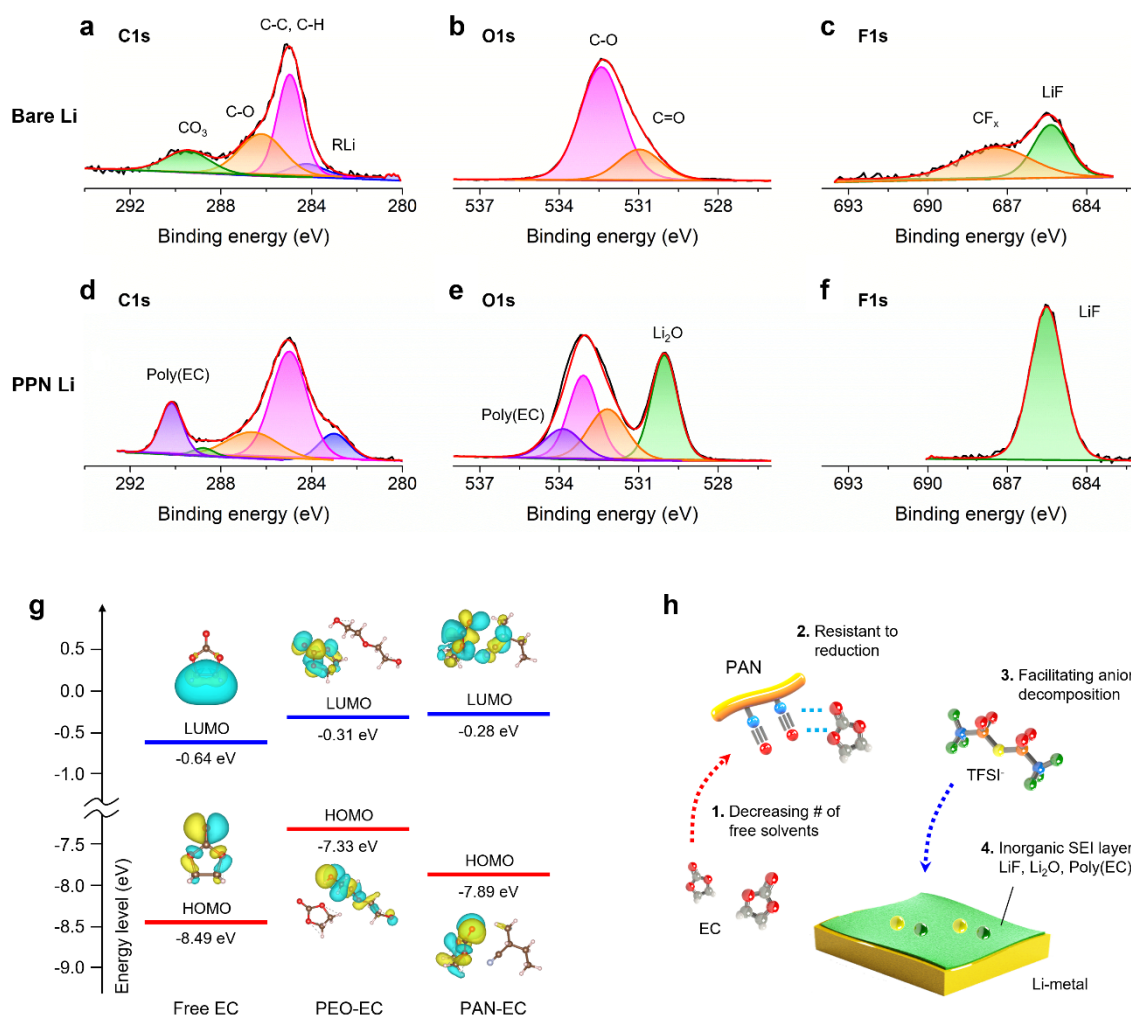


Fig. 4 Investigation of SEI layer on the cycled Li-metal. (a, d) XPS spectra of C1s, (b, e) O1s and (c, f) F1s for (a-c) bare Li and (d-f) PPN Li. The XPS were taken after Ar sputtering for 90 sec. (g) LUMO/HOMO levels of EC with different coordination: free EC, PEO-EC and PAN-EC. (h) Schematic illustration of the possible effects of PAN-EC interaction on SEI layer.

even initial deposition on the bare Li depicts a high-surface-area due to the porous nature from dendrites while relatively larger chunk of Li was observed on PPN Li (Fig. S5, ESI[†]).

The evolution of Li morphology was further investigated by *in-situ* optical microscopy. By such method, clear trends of Li-dendrite growth can be observed due to the removal of the separator which could act as a physical barrier (The detailed preparation process of *in-situ* observation cell can be found in Fig. S6, ESI[†]). The bare Li formed a notable amount of dendrites even after the 1st cycle (Fig. 3h). Apparently, the height of this porous layer rapidly increases from 110 μm (1st cycle) to over 400 μm (20th cycle). Assuming a flat plating, the theoretical height of utilized Li should be 4.39 μm per cycle, which suggests that the bare Li surface produces a highly porous Li during the repeated plating/stripping process. On the contrary, PPN Li demonstrated a much denser Li surface even after 20th cycle, probing Li-dendrites were successfully suppressed by PPN (Fig. 3i). The distance between the two Li electrodes after cycling also demonstrates that the PPN renders a stable Li plating/stripping while bare Li cell was short-circuited due to

the large amount of porous Li (Fig. S7, ESI[†]). In addition, the high reactivity of the carbonate electrolyte also causes a serious reaction with bare Li, which generates considerable gaseous byproducts (Fig. S8, ESI[†]).

In addition, the conductivities of LiTFSI : EC (1 : 6 molar ratio) in glass fiber and PPN layer (fabricated in the same liquid) were measured (Fig. S9, ESI[†]). We found that our PPN layer has a higher conductivity of $3.6 \times 10^{-3} \text{ S/cm}$ than liquid electrolyte, $1.3 \times 10^{-3} \text{ S/cm}$. We speculate that the polymer chains (cross-linked PEGDA) in PPN layer can work as an active Li⁺ ion conductor where ether group (C-O-C) can coordinate with Li⁺ through which Li ion may transport. Therefore, this fast and uniform Li⁺ ion flux may also result in low overpotential (Fig. 3a-c) and dense Li morphology (Fig. 3d-i) during Li plating/stripping.

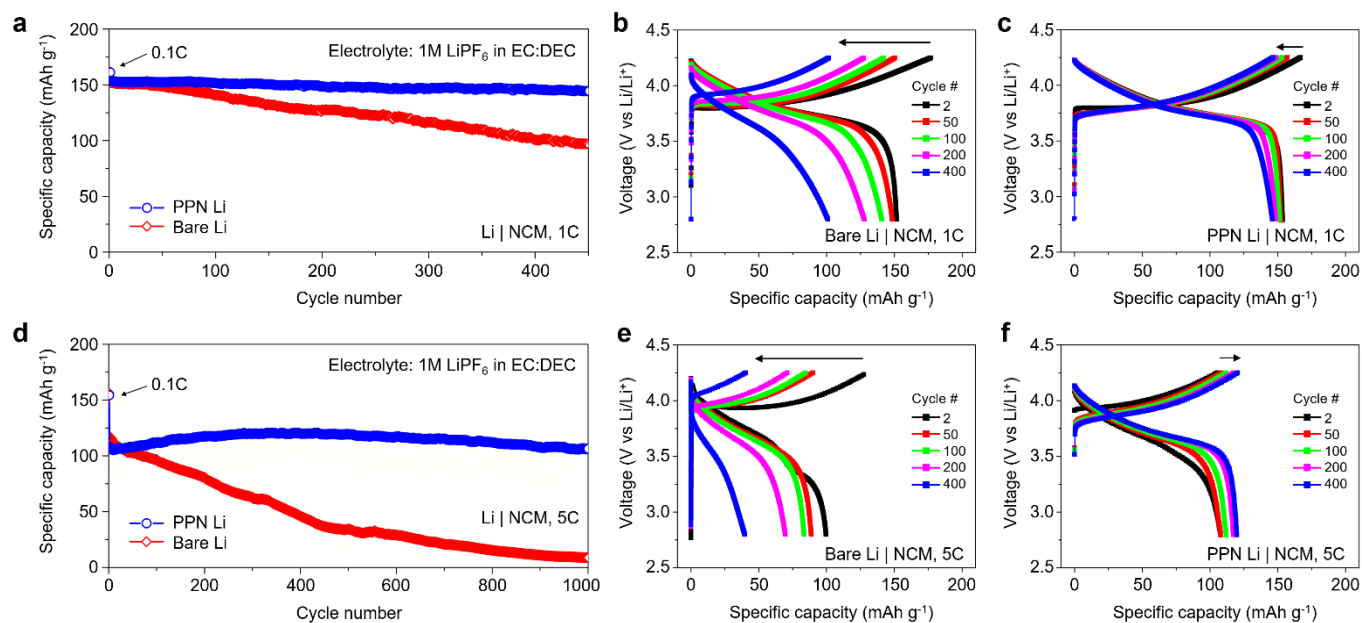


Fig. 5 Electrochemical performance of Li | NCM batteries. (a) Li | NCM battery cycling performance at 1C with bare Li (red) and PPN Li (blue). Voltage profiles during the cycling at 1C with (b) bare Li and (c) PPN Li. (d) Li | NCM battery cycling performance at 5C with bare Li (red) and PPN Li (blue). Voltage profiles during the cycling at 5C with (e) bare Li and (f) PPN Li. Li | NCM cells were cycled between 2.8 V to 4.25 V in 1M LiPF₆ in EC : DEC.

Composition of SEI layer on cycled Li-metal

The composition of the SEI layer was investigated by conducting X-ray photoelectron spectroscopy (XPS) on the Li-metal collected from symmetric Li | Li coin cells cycled 10 times under 5 mA cm⁻² (Fig. 4). The prepared samples were etched by Ar sputtering for 90 sec to eliminate the surface contamination (XPS spectra before sputtering can be found in Fig. S10, ESI†). In C1s spectra of bare Li, C-Li peak (283 eV), C-C/C-H peak (285 eV) along with C-O (287 eV), and CO₃ (288.5 eV) were observed, which are typical components for SEI layer such as lithium carbide, lithium alkyl carbonate or lithium carbonate (Li₂CO₃) from solvent-induced SEI formation (Fig. 4a). Similarly, O1s spectra of bare Li in Fig. 4b shows a strong C-O (532.5 eV) and C=O peaks (531 eV). In F1s spectra of bare Li in Fig. 4c, CF_x peak (689.5 eV) was found along with LiF (685.5 eV). However, the intensity of LiF peak was comparable to that of CF_x. From the XPS results, it can be speculated that the high reactivity of EC results in mostly organic but less inorganic segments in the SEI layer, which is readily soluble in the electrolyte and cannot effectively stabilize Li-metal.

PPN Li demonstrates much different compositions in the SEI layer. In C1s spectra, typical organic components were also observed but with much smaller intensity (Fig. 4d). Interestingly, an additional poly(EC) peak (290.5 eV) was found which is the product of polymerization of EC instead of the reduction,^{12, 16} which was also observed in O1s spectra around 534 eV (Fig. 4e). It is reported that poly(EC) is a flexible and stable SEI component to protect Li-metal against electrolyte attack.²⁵ In addition, O1s spectra also shows abundant Li₂O (529 eV) implying that the SEI layer on PPN Li is a thin and compact

layer compared with that of bare Li since Li₂O is known to form on the very surface of Li.²⁶ Most importantly, a strong LiF peak (685.5 eV) was observed on PPN Li as shown in F1s spectra (Fig. 4f). It is believed that salt anions (TFSI⁻) in PPN contribute more to the SEI layer formation than TFSI of bare Li, represented by such strong LiF peak.¹⁵

The lowest unoccupied molecular orbital (LUMO) and highest occupied molecular orbital (HOMO) levels of EC molecules with different coordination have been calculated since LUMO levels are related to the electrochemical reduction potential (Fig. 4g). The free EC molecule, which is not coordinated, has the lowest LUMO level (-0.64 eV) indicating it will be readily reduced by Li-metal during cycling. It is also possible that abundant free EC can coordinate with Li⁺, which is also easily reduced by Li-metal. More organic components in the SEI layer of bare Li can be expected by this low LUMO level of a redundant free EC molecules in carbonate electrolytes. By contrast, when EC is coordinated with PAN, it shows the highest LUMO level (-0.28 eV) which is higher than PEO-EC coordination (-0.31 eV) or free EC (-0.64 eV). Considering the low LUMO level (-0.52 eV) of pure PAN which is easily reduced by Li-metal, this high LUMO level (-0.28 eV) of PAN-EC interaction possibly makes PAN more difficult to be reduced as well (Fig. S11 and S12, ESI†).

Observations from the XPS data and LUMO level of the PPN Li surface confirm our hypothesis that PPN effectively regulates SEI layer on Li-metal. In Fig. 4h, possible effects of PPN are described. First, PAN-EC interaction decreases the number of free carbonate solvents on Li-metal, that will reduce the amount of organic component in the SEI layer which may enhance the chemical stability of the interphase. Second, the PAN-EC interaction makes both PAN and EC more difficult to be

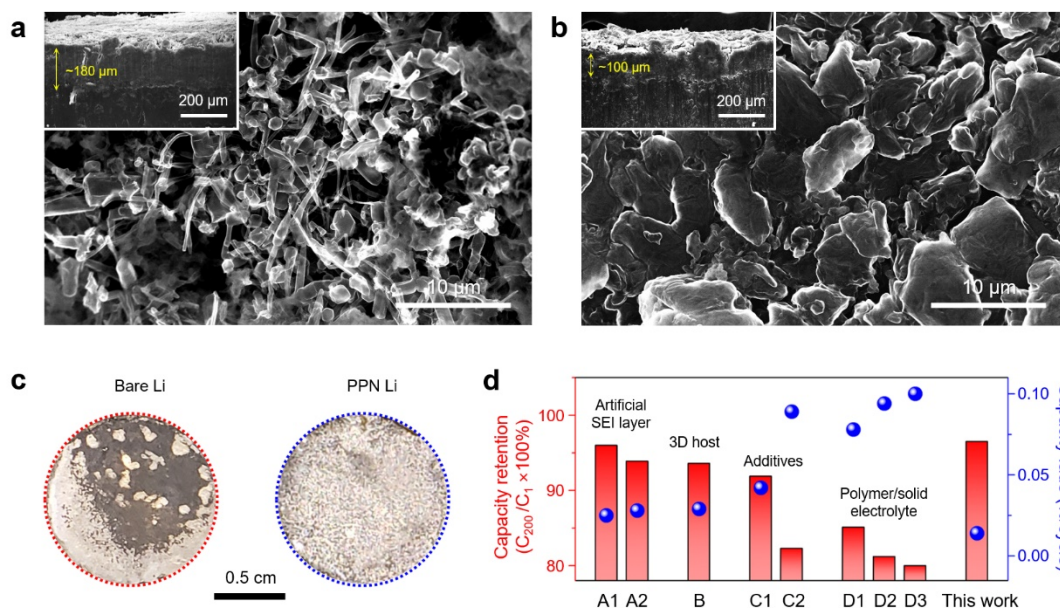


Fig. 6 Morphology of Li after electrochemical test. SEM images of Li surface from the Li | NCM cells after 1000 cycles at 5C with (A) bare Li and (B) PPN Li. The inset shows the cross-section SEM images indicating the utilized Li. (C) Photographs of Li-metal collected after cycling test with bare Li (left) and PPN Li (right). (D) Cycling stability comparison for recent studies of Li-metal batteries based on NCM cathode with various strategies. Red square charts show capacity retentions after 200 cycles (C_{200} = capacity after 200 cycles, C_1 = initial capacity) while blue dotted charts show capacity fade rate (%) per cycle. A1 and A2 denote artificial SEI layers.^{9, 10} B denotes 3D host for Li-metal.⁹ C1 and C2 denote electrolyte additives.^{13, 30} D1-D3 denote gel polymer, polymer, and inorganic electrolyte, respectively.³¹⁻³³ Capacity retentions of D2 and D3 were estimated from the capacity fade rate during 100 and 120 cycles, respectively.

reduced, and thus mitigating solvent decomposition. Third, PPN does not interact with salt anion, and thereby facilitating anion decomposition into inorganic SEI components. Combining these features, a stable SEI layer can be formed on Li-metal with abundant inorganic components such as LiF and Li₂O that can prevent electron transfer while allowing Li⁺ ion transport.²⁷ A significant amount of poly(EC), on the other hand, can serve as a flexible network that helps reinforce brittle inorganic components.^{25, 28} Note that the PPN during this SEI formation process (Fig. 4h) only guides electrolyte components (i.e., salt cation/anion and carbonate solvent) to form a stable SEI layer, but is not involved any electrochemical reaction, implying that the strategy used in this study is highly reliable and sustainable.

Electrochemical performance of Li | NCM cell

To verify the effectiveness of PPN Li in practical application, Li | NCM batteries with conventional electrolyte (1M LiPF₆ in EC : DEC) have been investigated without any additives. The cycling performance at 1C charge and 1C discharge (1C = full discharge in 1 hour) are presented in Fig. 5a. A formation cycle was conducted prior to the subsequent cycling test at C/10 where both bare Li and PPN Li shows an initial specific discharge capacity of ~160 mAh g⁻¹. In the latter cycles, the bare Li exhibits a rapid capacity fade with a capacity retention of 64% after 450 cycles at 1C. Such fast capacity fade can be attributed to the increased cell impedance from a combined effect of a highly resistive SEI layer and a depletion of electrolyte Li which may

adversely affect the transport of Li⁺ ions as well as interfacial kinetics (Fig. 5b).²⁹ On the contrary, PPN Li demonstrates a much improved cyclability with an improved capacity retention of 94% after 450 cycles at 1C (Fig. 5a). In the meantime, there is only subtle change in overpotentials over 400 cycles with PPN Li as shown in Fig. 5c, confirming that Li-metal has been effectively stabilized.

In addition, the cycling test under a higher current density (5C charge 5C discharge) was conducted with Li | NCM cells to further understand the role of PPN Li in a fast Li plating/stripping condition (Fig. 5d). The bare Li shows more drastic capacity fade which eventually leads to a cell failure after 1000 cycles at 5C (capacity retention of ~7.6%). The voltage profile of bare Li cell in Fig. 5e clearly indicates that the overpotential increases as the cell cycled, which is accompanied by a rapid capacity fade. On the other hand, PPN Li demonstrated a remarkably enhanced cyclability with an excellent capacity retention of 98.7% over 1000 cycles. It should be noted that not only was the cell discharged, but it was also charged under a high current density (5C, ~1.25 mA cm⁻²), which is a harsh condition that Li-metal can tolerate because a rapid volume expansion of Li-metal can physically and chemically damage SEI layer, which accelerates the growth of dendritic and dead Li. Taking this into account, our PPN Li significantly improved Li plating behavior over bare Li under a higher current density, which well coincides with symmetric Li | Li performance in Fig. 3a-c. The rate performance of Li | NCM cells was also investigated with bare Li and PPN Li (Fig. S13, ESI[†]) showing that PPN Li exhibits comparable rate capability to bare

Li. It is believed that the high conductivity of PPN layer (Fig. S9, ESI[†]) minimized the additional ohmic resistance caused by PPN layer. In summary, Li | NCM cell tests indicate that our PPN Li greatly improved electrochemical performance of Li-metal batteries in conventional carbonate electrolyte (1M LiPF₆ in EC : DEC) under a high current density (> 1 mA cm⁻²). The superior performance of PPN Li can be also observed in single-solvent electrolyte (LiTFSI : EC = 1 : 6) with an improved cycling stability as well as a rate performance (Fig. S14 and S15, ESI[†]).

The different interfacial chemistry often results in divergent morphology of Li during the cycling. Figure 6a and 6b show the SEM images of Li surface obtained from Li | NCM cells after 1000 cycles at 5C for bare Li and PPN Li, respectively. The bare Li in a typical carbonate-based electrolyte generated thin and long Li, namely, whisker-like Li or Li-dendrite (Fig. 6a). The surface of Li is highly porous with a high-surface-area (See Fig. S16 for the SEM image of porous Li, ESI[†]). This dendritic morphology is indicative of poor cycling stability of bare Li | NCM cells since the dead Li can accumulate and increase the diffusion length for Li⁺ ions. It is also interesting that Li morphology is different when different electrolyte is used such as LiTFSI : EC (Fig. 3) and 1M LiPF₆ in EC : DEC (Fig. 6). It is believed that relatively low concentration in Li | NCM cell resulted in more dendritic and porous Li buildup. Note that despite the formation of Li-dendrites shown in Fig. 6a, the Li | NCM cell with bare Li showed only a rapid capacity fade, but not short-circuiting (Fig. 5a and d). With larger pores of glass fiber, however, the bare Li cell was eventually short-circuited after 200 cycles while PPN Li exhibits a stable cycling (Fig. S17, ESI[†]). Interestingly, a notably different morphology was observed on PPN Li (Fig. 6b). Unlike highly porous and dendritic Li from bare Li, PPN Li renders much denser Li chunks with a low-surface-area. It is believed that a stable interface between Li and PPN leads to uniform deposition of Li with a dense morphology. The insets of Fig. 6a and 6b indicate that bare Li results in a buildup of thick dead Li (~180 μm) while PPN Li shows thinner Li utilization (~100 μm). The photographs of Li-metals, that were collected after the cell test with NCM, clearly reveal that bare Li has abundant dead Li on the surface (dark area) while PPN Li shows no notable dead Li, which is represented by a relatively clean and uniform Li surface (Fig. 6c).

The ability to stabilize Li-metal can be evaluated by comparing the cycling stability of a full cell. The accumulation of the dead Li and SEI on the Li-metal surface causes an increase in the cell impedance, short-circuits or drying of the electrolyte, which is reflected by decreasing discharge capacity during the cycling. In Fig. 6d, the cycling stability of recent studies based on Li-metal batteries with NCM cathode is compared (See Table S1 for details, ESI[†]). The PPN Li employed in this work exhibits the highest capacity retention (96.5%) after 200 cycles among various strategies such as artificial SEI layers (A1⁹ and A2¹⁰), 3D host (B⁸), electrolyte additives (C1³⁰ and C2¹³) or polymer/solid electrolytes (D1,³¹ D2³² and D3³³). In addition, the PPN Li demonstrates the lowest capacity fade rate of 0.013% over 450 cycles while the previous studies show a capacity fade rate of 0.025% per cycle at most (i.e., A1).⁹ It is noteworthy that the cycling performances of most previous studies (A1, A2, B, C1

and C2) were obtained with the help of electrolyte additives, such as 1~2 wt% of fluoroethylene carbonate (FEC),⁹ vinylene carbonate (VC)^{8, 9} or lithium nitrate (LiNO₃).¹³ Therefore, the strategy used in this study, that the restriction of carbonates by the polymer-solvent interaction, shows a superior ability to stabilize Li-metal in carbonate electrolyte even without electrolyte additives.

Conclusions

An effective approach to inhibit the high reactivity of carbonates in Li-metal batteries has been developed by controlling the polymer-solvent interactions. While bare Li generates a significant amount of Li-dendrite and dead Li, the PPN protective layer can stabilize Li-metal surface without notable dendrites on the surface of Li. The PPN protective layer not only confines the carbonate solvents, but also facilitates anion contribution to the SEI layer that has a high content of inorganic components. The stabilized interface formed between Li and PPN enables a sustainable plating/stripping of Li under high current density and also prevents further reaction of Li with electrolyte improving cycling stability of Li-metal batteries. These key findings of PPN for Li-metal represent a useful perspective to understand and improve interfacial chemistry of electrolyte and Li-metal for future applications in rechargeable batteries.

Author contributions

G.Y. supervised the project. J.B., Y.L., and G.Y. conceived the idea and co-wrote the manuscript. Y.Q. performed simulation work. J.B. and X.Z. performed materials fabrication and characterization. J.B. carried out data analysis. All authors discussed the results and commented on the manuscript.

Conflicts of interest

The authors declare no competing financial interests.

Acknowledgements

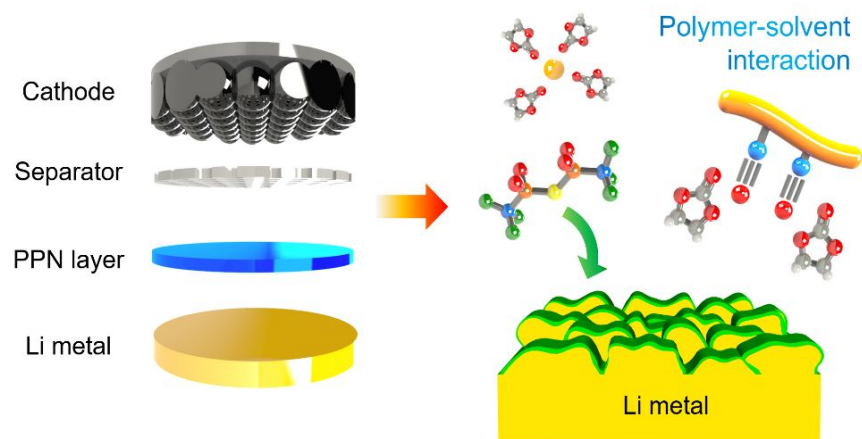
G.Y. acknowledges the funding support from the Center for Mesoscale Transport Properties, an Energy Frontier Research Center supported by the U.S. Department of Energy, Office of Science, Basic Energy Sciences, under Award #DE-SC0012673, as well as Camille Dreyfus Teacher-Scholar Award.

Notes and references

1. J. M. Tarascon and M. Armand, *Nature*, 2001, **414**, 359.
2. D. Lin, Y. Liu and Y. Cui, *Nat. Nanotechnol.*, 2017, **12**, 194.
3. X.-B. Cheng, R. Zhang, C.-Z. Zhao and Q. Zhang, *Chem. Rev.*, 2017, **117**, 10403-10473.
4. W. Zhou, S. Wang, Y. Li, S. Xin, A. Manthiram and J. B. Goodenough, *J. Am. Chem. Soc.*, 2016, **138**, 9385-9388.

5. X. Han, Y. Gong, K. K. Fu, X. He, G. T. Hitz, J. Dai, A. Pearse, B. Liu, H. Wang, G. Rubloff, Y. Mo, V. Thangadurai, E. D. Wachsman and L. Hu, *Nat. Mater.*, 2017, **16**, 572-579.
6. J. Bae, Y. Li, J. Zhang, X. Zhou, F. Zhao, Y. Shi, J. B. Goodenough and G. Yu, *Angew. Chem. Int. Ed.*, 2018, **57**, 2096-2100.
7. K. Xu, *Chem. Rev.*, 2014, **114**, 11503-11618.
8. C. Niu, H. Pan, W. Xu, J. Xiao, J.-G. Zhang, L. Luo, C. Wang, D. Mei, J. Meng, X. Wang, Z. Liu, L. Mai and J. Liu, *Nat. Nanotechnol.*, 2019, **14**, 594-601.
9. M. S. Kim, J.-H. Ryu, Deepika, Y. R. Lim, I. W. Nah, K.-R. Lee, L. A. Archer and W. Il Cho, *Nat. Energy*, 2018, **3**, 889-898.
10. Y. Gao, Z. Yan, J. L. Gray, X. He, D. Wang, T. Chen, Q. Huang, Y. C. Li, H. Wang, S. H. Kim, T. E. Mallouk and D. Wang, *Nat. Mater.*, 2019, **18**, 384-389.
11. Q. Pang, X. Liang, A. Shyamsunder and L. F. Nazar, *Joule*, 2017, **1**, 871-886.
12. J. Zheng, M. H. Engelhard, D. Mei, S. Jiao, B. J. Polzin, J.-G. Zhang and W. Xu, *Nat. Energy*, 2017, **2**, 17012.
13. Y. Liu, D. Lin, Y. Li, G. Chen, A. Pei, O. Nix, Y. Li and Y. Cui, *Nat. Commun.*, 2018, **9**, 3656.
14. K. N. Wood, E. Kazyak, A. F. Chadwick, K. H. Chen, J. G. Zhang, K. Thornton and N. P. Dasgupta, *ACS Cent. Sci.*, 2016, **2**, 790-801.
15. D. Aurbach, E. Pollak, R. Elazari, G. Salitra, C. S. Kelley and J. Affinito, *J. Electrochem. Soc.*, 2009, **156**, A694-A702.
16. V. Sharova, A. Moretti, T. Diemant, A. Varzi, R. J. Behm and S. Passerini, *J. Power Sources*, 2018, **375**, 43-52.
17. D. Aurbach, Y. Gofer, M. Ben-Zion and P. Aped, *J. Electroanal. Chem.*, 1992, **339**, 451-471.
18. Q. Y. Wu, X. N. Chen, L. S. Wan and Z. K. Xu, *J. Phys. Chem. B*, 2012, **116**, 8321-8330.
19. D. W. McOwen, D. M. Seo, O. Borodin, J. Vatamanu, P. D. Boyle and W. A. Henderson, *Energy Environ. Sci.*, 2014, **7**, 416-426.
20. D. Ostrovskii, A. Brodin, L. M. Torell, G. B. Appetecchi and B. Scrosati, *J. Chem. Phys.*, 1998, **109**, 7618-7624.
21. J. Li, X. Huang and L. Chen, *J. Electrochem. Soc.*, 2000, **147**, 2653-2657.
22. Y. Yamada, K. Furukawa, K. Sodeyama, K. Kikuchi, M. Yaegashi, Y. Tateyama and A. Yamada, *J. Am. Chem. Soc.*, 2014, **136**, 5039-5046.
23. S.-K. Jeong, H.-Y. Seo, D.-H. Kim, H.-K. Han, J.-G. Kim, Y. B. Lee, Y. Iriyama, T. Abe and Z. Ogumi, *Electrochem. Commun.*, 2008, **10**, 635-638.
24. J. Qian, W. A. Henderson, W. Xu, P. Bhattacharya, M. Engelhard, O. Borodin and J. G. Zhang, *Nat. Commun.*, 2015, **6**, 6362.
25. J. Zheng, P. Yan, D. Mei, M. H. Engelhard, S. S. Cartmell, B. J. Polzin, C. Wang, J.-G. Zhang and W. Xu, *Adv. Energy Mater.*, 2016, **6**, 1502151.
26. E. Peled, D. Golodnitsky and G. Ardel, *J. Electrochem. Soc.*, 1997, **144**, L208-L210.
27. X. Q. Zhang, X. Chen, X. B. Cheng, B. Q. Li, X. Shen, C. Yan, J. Q. Huang and Q. Zhang, *Angew. Chem. Int. Ed.*, 2018, **57**, 5301-5305.
28. C. Yan, X.-B. Cheng, Y. Tian, X. Chen, X.-Q. Zhang, W.-J. Li, J.-Q. Huang and Q. Zhang, *Adv. Mater.*, 2018, **30**, 1707629.
29. J. Bae, Y. Li, F. Zhao, X. Zhou, Y. Ding and G. Yu, *Energy Storage Mater.*, 2018, **15**, 46-52.
30. J. Alvarado, M. A. Schroeder, T. P. Pollard, X. Wang, J. Z. Lee, M. Zhang, T. Wynn, M. Ding, O. Borodin, Y. S. Meng and K. Xu, *Energy Environ. Sci.*, 2019, **12**, 780-794.
31. H. Duan, M. Fan, W.-P. Chen, J.-Y. Li, P.-F. Wang, W.-P. Wang, J.-L. Shi, Y.-X. Yin, L.-J. Wan and Y.-G. Guo, *Adv. Mater.*, 2019, **31**, 1807789.
32. F.-Q. Liu, W.-P. Wang, Y.-X. Yin, S.-F. Zhang, J.-L. Shi, L. Wang, X.-D. Zhang, Y. Zheng, J.-J. Zhou, L. Li and Y.-G. Guo, *Sci. Adv.*, 2018, **4**, eaat5383.
33. J.-Y. Liang, X.-X. Zeng, X.-D. Zhang, T.-T. Zuo, M. Yan, Y.-X. Yin, J.-L. Shi, X.-W. Wu, Y.-G. Guo and L.-J. Wan, *J. Am. Chem. Soc.*, 2019, **141**, 9165-9169.

Table of contents



Effective and dense Li plating/stripping by suppressing free solvents from intermolecular dipole-dipole interaction between polar polymer & solvents, resulting in high-performance Li-metal batteries.